

Lévy Stable Law Description of the Intermittent Behavior in Pb+Pb Collisions at 158 AGeV/c

A.M. Tawfik and E. Ganssauge

FB Physik, Marburg University, Renthof 5, D-35032 Marburg, Germany

Abstract

The factorial moments (FM) of multiplicity distributions in one- and two-dimensions are studied for Pb+Pb collisions at 158 AGeV/c. The results are compared with FRITIOF, RQMD and VENUS predictions. In the relation between FM and the number of partitions, M , obvious *positive* intermittence exponents, ϕ_q , are observed. The exponents, ϕ_q , are compared with the anomalous dimensions, d_q . Then they are expressed in terms of Lévy stable indices, μ . Meanwhile the experimental data within the interval, $2 < \eta < 6$, fulfills the requirements of the Lévy stable region ($0 \leq \mu \leq 2$), the results from the other intervals are away from this region. All their corresponding indices have negative values.

PACS: 25.75.G, 61.43, 12.38.M, 64.60.Q

1 Introduction

Since the observations of JACEE collaboration [1] and the pioneer works of Bailas and Peschanski [2, 3] around mid of 1980's, the intermittent behavior in multi-particle production has increasingly gained full credibility among the high-energy physicists. The concept "intermittence" itself is primarily used to describe the fluctuations observed in the particle density distributions. In many experiments, the *large dynamic* fluctuations at the final state of particle production has been confirmed. To get a satisfactory explanation for the power-law behavior of FM with the partition number, M , many theoretical approaches are proposed. For example, self-similar branching, QCD parton cascade, multi-particle cascade, second-order phase-transition, etc. Also the effects of Bose-Einstein correlations on the two-particle correlation functions [4, 5, 6, 7] may explain this behavior. The randomization and the hadronic Čerenkov radiation are suggested to be partially responsible for such power-scaling behavior. Also, if QGP has been produced, the effects of the soft and hard collisions, the clustering and resonance decay and the showering in the QGP-surrounding manifest themselves in forms of: multiplicity fluctuation, power-scaling behavior, self-

similar branching, jet structure, etc. Some of these effects are responsible for a kind of *canonical* fluctuations in the particle production.

In this paper, the behavior of FM is studied for Pb+Pb collisions at 158 AGeV/c with successive partitions in one- (pseudo-rapidity η or azimuthal angles $\phi \in \{0, 2\pi\}$), and two-dimensions (η and ϕ). The produced particles are classified into four groups according to their pseudo-rapidity values ($3 < \eta < 4$, $3 < \eta < 5$, $2 < \eta < 5$ and $2 < \eta < 6$). The observed intermittence exponents, ϕ_q , are compared with the anomalous dimensions, d_q (Rényi dimensions, \mathcal{R}_q). After that, they are plotted in the Lévy space.

This article is organized as the following: The experimental material and the simulation by using the three events generators, FRITIOF, RQMD and VENUS are complemented in Section 2. The definitions and formalism are given in Section 3. The results of FM and the intermittence exponents, ϕ_q , in one- and in two-dimensions are introduced in Sections 4 and 5, respectively. The relations between the intermittence and the anomalous exponents and their expressions in terms of Lévy indices, μ , are discussed in Section 6. Section 7 contains some remarks and the final conclusions.

2 Experimental Material

The data used in this paper is retrieved from some of the Pb-chambers irradiated at CERN-SPS during 1996 for the EMU01 collaboration. This material was consummately measured and analyzed at the Marburg University by using our measuring system MIRACLE Lab [8, 9, 10]. The collisions have been recorded with ^{82}Pb -beam accelerated to incident momentum of 158 AGeV/c and then fired towards stationary lead foil with thickness $\sim 250 \mu\text{m}$. The lead foil was positioned in the front of seven consecutively arranged plastic sheets coated on both sides by the nuclear emulsion, FUJI ET-7B. Because of the relatively high transverse momentum, most of, if not all, produced particles and fragmentations are emitted within a narrow forward cone. Therefore, their tracks can be registered within the forward emulsion sheets. The exposure process is mainly controlled by counting the heavily ionizing particles by using scintillator and discriminator with relatively high threshold settings. The number of beam-particles is registered by using an additional counter installed behind the emulsion chamber. Scale and driver electronics (CAEN N145) are used to build up pulses to be transferred to the SPS-“kicker” magnet. The kicker magnet consequently removes the beam, if the particle number transcends 3000 per spot. The beam density is $\sim 5 \cdot 10^2$ nuclei/cm².

The scanning efficiency in the emulsion chambers is 0.75 ± 0.05 [11]. The emulsion sensitivity for singly charged particles is as good as 30 grains per 100 μm . Depending on the incident momentum, the polar angle can be calculated. For the actual data, we get polar angle of 1.3 mrad. Depending on topology of the microscope’s field of view, particles with space angles, $\theta < 30^\circ$ ($\eta = -\ln \tan(\theta/2) > 1.32$) can be acquired. Obviously, most of produced parti-

cles are singly charged. It is expected that they are mixed with contamination of $e^- - e^+$ pairs from Dalitz decay and γ -conversion. The possible *overestimation* of the observed particles density has been determined as $\sim 2\%$ [8]. As a reason of the reconstruction algorithm [10] applied for the measuring system MIRACLE Lab, the tracks of these electrons are *completely* disregarded. In comparison with *human* operators, it is found that MIRACLE Lab has an efficiency up to 96% [10]. Large part of this 4% discrepancy is obviously coming from the particles emitted with large space angles ($\theta \geq 30^\circ$). The missing measurements, frequent scattering, unresolved close-pairs and pair production represent additional sources for this discrepancy [9]. Therefore, we could consciously suggest to renounce the discussion of the effects of γ -conversion on FM (see Section 4.2 and Section 5.3 for more details).

2.1 Simulation of the experimental data

The investigation of FM is performed for the collisions with restricted particle multiplicity¹ ≥ 1200 . From these events, only the particles emitted within predefined pseudo-rapidity intervals ($3 < \eta < 4$, $3 < \eta < 5$, $2 < \eta < 5$ and $2 < \eta < 6$) are taken into account. These η -intervals are chosen at and around the mid-rapidity region. Due to the chiral symmetry breaking, the produced particles are mainly pions, π 's. Therefore, the restriction on the η -values is necessary to study the phase-transition, which, in turn, should be restricted to the produced particles only. Therefore, the narrow η -intervals are the suitable ones to study the produced particles and consequently the phase-transition. Once again, here we used another restriction on the considered phase-space.² On the azimuthal angles, there is no restriction at all, (for each $\Delta\eta$ group, the considered ϕ -window is allowed to take any real value within the available spectrum, $\{0, 2\pi\}$).

For the event generators FRITIOF 7.02 [13], RQMD 2.1 [14] and VENUS 4.12 [15], the input parameters are adjusted for the destination to produce simulated events with total multiplicity not smaller than 1200. Each simulated event has to go through different cutting processes, in order to simulate, as good as possible, the “real” events (Section 2). After these operations, the number of particles observed within the space angle, $\theta < 30^\circ$, has to be ≥ 1200 . The criteria used for the data cutting, can be taken from [8, 9, 10]:

1. $\beta = \vec{p}/E > 0.7$. In practice, we can mainly measure singly charged particles. More than 90% of them are charged π 's. The number of highly charged particles is relatively small [11].
2. $\eta = -\ln \tan(\theta/2) > 1.32$. The space angle is restricted within $\theta < 30^\circ$ depending on the geometry of the emulsion chamber, and of the microscope's field of view.

¹ This is a restriction on the multiplicity (see Section 3 for the effects of the multiplicity restriction on FM [12])

² The influences of the restriction on the considered phase-space to get *flat* distributions of FM are discussed in Section 3.

3. Charged particles. The emulsion is sensitive for the charged particles only.

3 Definitions and Formalism

If the phase-space, $\Delta\eta$, is split into M bins of equal sizes, $\delta\eta = \Delta\eta/M$, the *exclusive* scaled factorial moments [2, 3] are given as

$$F_q(M)^{\text{excl}} = M^{q-1} \sum_{m=1}^M \frac{\langle n_m(n_m-1)\cdots(n_m-q+1) \rangle}{\bar{n}(\bar{n}-1)\cdots(\bar{n}-q+1)}, \quad (1)$$

n_m is the multiplicity in m -th bin and \bar{n} is the average multiplicity in the whole $\Delta\eta$ -window. With successive partition, $\Delta\eta \rightarrow 0$, a power-law scaling can describe the fluctuations in the particle production,

$$F_q(M) = M^{q-1} \frac{\sum_{m=1}^M \prod_{i=1}^q \int_{\eta_{m-1}}^{\eta_m} d\eta_i \rho_n^{(q)}(\eta_1, \eta_2, \dots, \eta_q)}{\prod_{i=1}^q \int_{\eta_0}^{\eta_0+\Delta\eta} d\eta_i \rho_n^{(q)}(\eta_1, \eta_2, \dots, \eta_q)}, \quad (2)$$

$\rho_n^{(q)}(\dots)$ is the pseudo-rapidity density in a sub-interval with q particles investigated in an event with n total multiplicity. η_0 is the minimum pseudo-rapidity in m -th bin and η_m is the pseudo-rapidity value in this bin ($\eta_m = \eta_0 + m \cdot \Delta\eta/M$). Then the factorial moments in m -th bin are to be given as

$$F_q(M) = \frac{\prod_{i=1}^q \int_{\eta_{m-1}}^{\eta_m} d\eta_i \rho_n^{(q)}(\eta_1, \eta_2, \dots, \eta_q)}{\prod_{i=1}^q \int_{\eta_0}^{\eta_0+\Delta\eta} d\eta_i \rho_n^{(q)}(\eta_1, \eta_2, \dots, \eta_q)}. \quad (3)$$

In the case that there is no correlation between the produced particles, FM, in the whole $\Delta\eta$ -interval, can be given as

$$F_q(M) = M^{q-1} \sum_{m=1}^M \left(\int_{\eta_{m-1}}^{\eta_m} d\eta_m \bar{P}_n(\eta) \right)^q, \quad (4)$$

$\bar{P}_n(\eta) = \rho_n(\eta)/\bar{n}$ is the normalized distribution of pseudo-rapidity density in a bin of with size η . When $\eta \rightarrow \Delta\eta$, we get the maximum value

$$F_q(M)^{\text{max}} = \Delta\eta^{q-1} \int_{\eta_0}^{\eta_0+\Delta\eta_m} d\eta [\bar{P}_N(\eta)]^q. \quad (5)$$

When $F_q(M)^{\text{max}} = 1$, the single-particle distribution in the $\Delta\eta$ -window will be a plane one³ (a distribution with non-statistical fluctuations).

³ A powerful method to produce *flat* particle density distributions from *non-flat* ones can be taken from [16].

In this section, we have discussed the *exclusive* FM and their limitations to describe the multiplicity fluctuations. In the next section, we pass to their possible applications to describe the particle production in heavy-ion collisions.

3.1 Factorial moments and intermittence exponents

For many reasons⁴, the direct calculation of the *exclusive* FM is not easy, especially for high statistics. Therefore, it has been suggested [2, 3, 18] to implement another kind of FM, namely the *inclusive* FM,

$$F_q(M)^{\text{incl}} = M^{q-1} \sum_{m=1}^M \frac{\langle n_m(n_m - 1) \cdots (n_m - q + 1) \rangle}{\bar{n}^q}. \quad (6)$$

The value, \bar{n} , is coming out by dividing the observed multiplicity by the bin number, M , and then by the number of events, N . The exclusive and inclusive FM are the same, if the particle production can be described by Poisson function. In principle, the particle density distribution depends on the dynamics of the interacting system (mass, energy, number of events, whether there is any restriction in the data sample,^e etc.).

$$F_q^{\text{incl}} = \frac{\bar{n}(\bar{n} - 1) \cdots (\bar{n} - q + 1)}{\bar{n}^q} \cdot F_q^{\text{excl}}. \quad (7)$$

Then in the real case, the difference between both types of FM is actually the long-range correlations, which appear as a reason of the strong effects of the multiplicity on the correlation functions [12, 19, 20].

By definition [2, 3, 18, 21], FM used in the particle production are

$$\langle F_q(M) \rangle = \left\langle \frac{\langle n_k(n_k - 1) \cdots (n_k - q + 1) \rangle}{\langle n_k \rangle^q} \right\rangle, \quad (8)$$

$\langle n_k \rangle$ is the average multiplicity in k -th bin of size $\delta\eta$. According to the *self-similar density fluctuations*, the successive partitions of the pseudo-rapidity, $\Delta\eta$, leads to the following power-law dependency

$$\langle F_q(M) \rangle \propto M^{\phi_q}. \quad (9)$$

The exponents, ϕ_q , are called the “intermittence exponents”, which practically can be retrieved from the slopes of the relations between $\log F_q$ and $\log M$. They are also related to the “anomalous dimensions” [22]

$$d_q = \frac{\phi_q}{q - 1}. \quad (10)$$

The fractal Rényi dimensions [23] are defined as functions of the “anomalous dimensions” d_q

⁴ Mainly, there are two reasons: the limitation on the considered pseudo-rapidity, in order to get flat particle density distributions and the limitation on multiplicity [17], in order to avoid any possible *dynamical* correlation between the produced particles.

$$\mathcal{R}_q = \mathcal{R} \cdot (1 - d_q), \quad (11)$$

The constant, \mathcal{R} , is the topological Rényi dimension. For *multi-fractal* processes, d_q can be given as functions of the orders, q , only (Section 6.3 and Section 6.4). For *mono-fractal* processes (Section 6), d_q are constant. Actually, Rényi dimensions can be used to measure the randomization in the produced particles. For the total randomization, $\phi_q = 0$, $d_q = 0$, and consequently $\mathcal{R}_q = \mathcal{R}$.

4 Results in One-Dimension

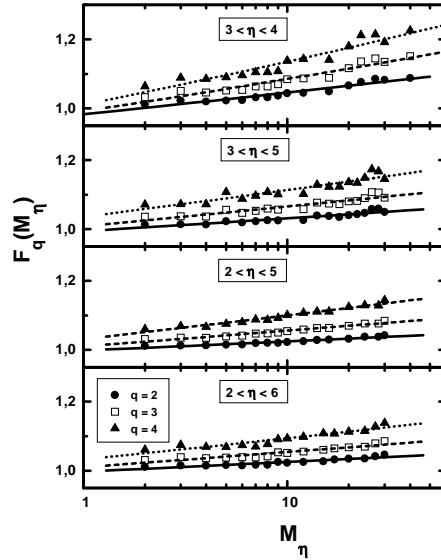


Figure 1: The factorial moments, F_q , for the orders, $q = \{2, 3, 4\}$, are plotted as functions of small partition number, M_η , in η -dimension. The data used here are Pb+Pb collisions at 158 AGeV/c with total multiplicity ≥ 1200 . The different $\Delta\eta$ -windows are applied above the whole region of pseudo-rapidity ($\eta > 1.32$). Only the secondary particles emitted within these windows are taken into consideration. The data are fitted as straight lines. Their slopes are the “intermittence exponents” ϕ_q .

In both “real” and “simulated” collisions, pseudo-rapidity intervals are successively split into M equal sub-intervals (bins). In each such bins, the multiplicity and then the corresponding q -order FM are calculated according to Eq. (8). Fig. 1 shows F_q as functions of M_η for the orders, $q = \{2, 3, 4\}$, and for the different $\Delta\eta$ -intervals given in Section 2.1. The underscore in M_η means that the partition has been performed in η -dimension. The splitting in the other dimension is completely avoided here. We notice that all pictures show obvious

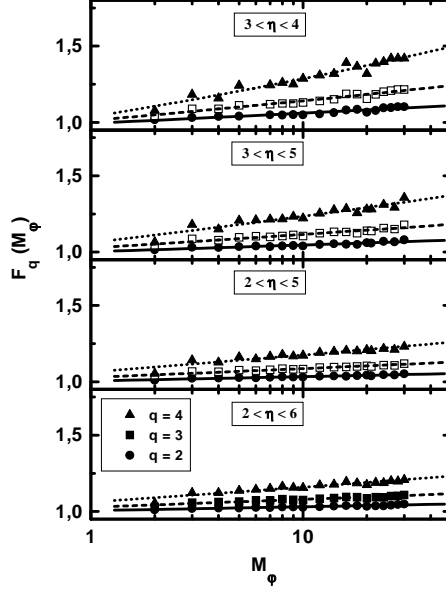


Figure 2: The factorial moments, F_q , for the orders, $q = \{2, 3, 4\}$, are plotted as functions of small partition number, M_ϕ , in ϕ -dimension. As in Fig. 1 the data are fitted as straight lines. Correspondingly their slopes give the component of “intermittence exponents” in ϕ -dimension, ϕ_q .

positive intermittence slopes, ϕ_q . Also, it is to realize that the FM-values increase with the decreasing of $\Delta\eta$ -intervals. Another remarkable finding noticed here is that the slopes increase with the increasing of the orders, q (review Eq. (8)). The analysis depicted in Fig. 2 is for the partition in ϕ -dimension. Nearly, the same qualitative features as in previous figure are noticed here. Through increasing the partition number, M_η or M_ϕ , the values of the corresponding FM raise fast, as shown in Fig. 3 and Fig. 4. The reasons for this upwards increasing will be discussed later (Section 4.1). For now, the discussion is restricted only on the phenomenological behavior of the increasing of FM with $M_{\{\eta|\phi\}}$. In Fig. 3, the smallest $\delta\eta$ in all pictures is ~ 0.01 , which seems to be coincident with the detector resolution. Beyond this value, FM reduce suddenly (not shown here), i.e. the upwards increasing of FM (shown here) gets inverted. This boundary limit can be taken as the low-value of the detector resolution. Until such point, we can effectively count the produced particles and then correctly calculate their FM. Beyond it, it is impossible to assure whether the measured particles are *real* ones and consequently their calculated FM must be associated with large statistical errors. The range of the linear dependence in Fig. 3 becomes larger with wider $\Delta\eta$ -windows. Some kind of plateau begin to appear with the increasing of $\Delta\eta$. Figure 4 depicts the same investigations as Fig. 3, but for the partition in the ϕ -dimension. Nearly, same qualitative features as in Fig. 3 are

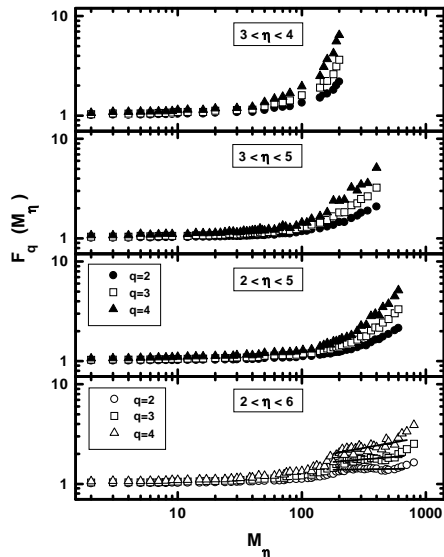


Figure 3: The factorial moments, F_q , for the orders, $q = \{2, 3, 4\}$, are depicted as functions of large partition number, M_η , in η -dimension. The partition process is repeated as long as the FM-values increase. An exponential growth of FM is noticed for relatively large M_η . Within the largest $\Delta\eta$ -interval, we notice that the increasing of FM is saturated.

noticed here. The only difference is that there is no plateau in any curvature region.

In addition to the large statistical errors, there are other reasons for the negative dependence of $F_q(M_{\{\eta|\phi\}})$ on large $M_{\{\eta|\phi\}}$: The properties of FM themselves. The FM used here can be applied, only if the following conditions are simultaneously fulfilled:

- The order q has an integer positive value.
- The multiplicity in each bin (n_m) is larger than or at least equal to q .
- q is greater than or at least equal to 2.

In Fig. 3 and Fig. 4, we could expect that the multiplicity, n_m , can be smaller than q . If the limit, $q < n_m$, has been reached, we cannot correctly implement Eq. (8). The discussion of FM for large $M_{\{\eta|\phi\}}$ should not, in the one hand, lead to the conclusion that we would like to go through any argumentation of the detector resolution. But, as we think, it is a *worthwhile* finding to realize that our measuring system MIRACLE Lab [8, 9, 10] is effectively able to determine the emulsion resolution. This efficiency has been estimated (for example, by testing its reproduction of the measured tracks, when the emulsion plates are

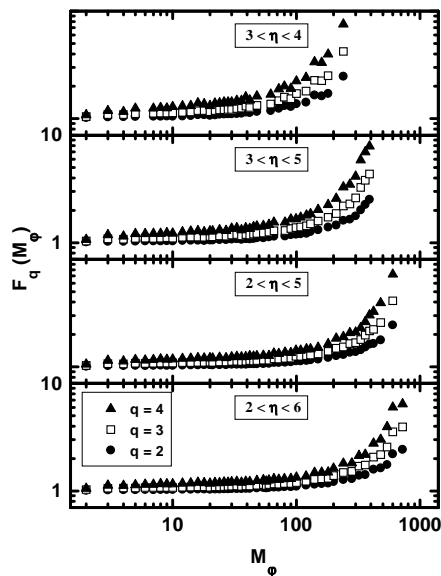


Figure 4: The factorial moments, F_q , for the orders, $q = \{2, 3, 4\}$, as functions of relatively large partition number, M_ϕ , in ϕ -dimension. As in Fig. 3 the partition process is repeated as long as the FM-values increase. Here there is no evidence for the saturation region.

randomly rotated). In the other hand, this discussion enabled us to refer to the limitations of the used FM.

The predictions from the three events generators are illustrated in Fig. 5. For FRITIOF simulation one notice that FM have non-linear dependencies for relatively small M_η . Also, the values of FM are not coincident with the experimental ones shown in Fig. 1. For large M_η , the upwards increasing is to be observed until bin size $\delta\eta \rightarrow 0.005$. Within these small bins, large numerical uncertainties in the computations are obviously expected. Therefore, these regions should be charily studied and no serious conclusions according to their features should be drawn. The saturation plateau here is too weak. Obviously, they begin later and have smaller width than the experimental ones (Fig. 2). From the results of RQMD calculations nearly the same features as in previous picture are observed. The width of the saturation plateau is larger than that in FRITIOF. Although the saturation regions of the VENUS calculations seem to be comparable with the corresponding regions in Fig. 2, they are still unable to completely predict the experimental results. Obviously, the different discrepancies between the experimental data and the three models become larger with increasing M_η (see Fig. 11, later). This may be explained due to the effects of Bose–Einstein correlations, which are not included in any model. In addition to this, during the experimental observations [24], these effects have not been considered. Another

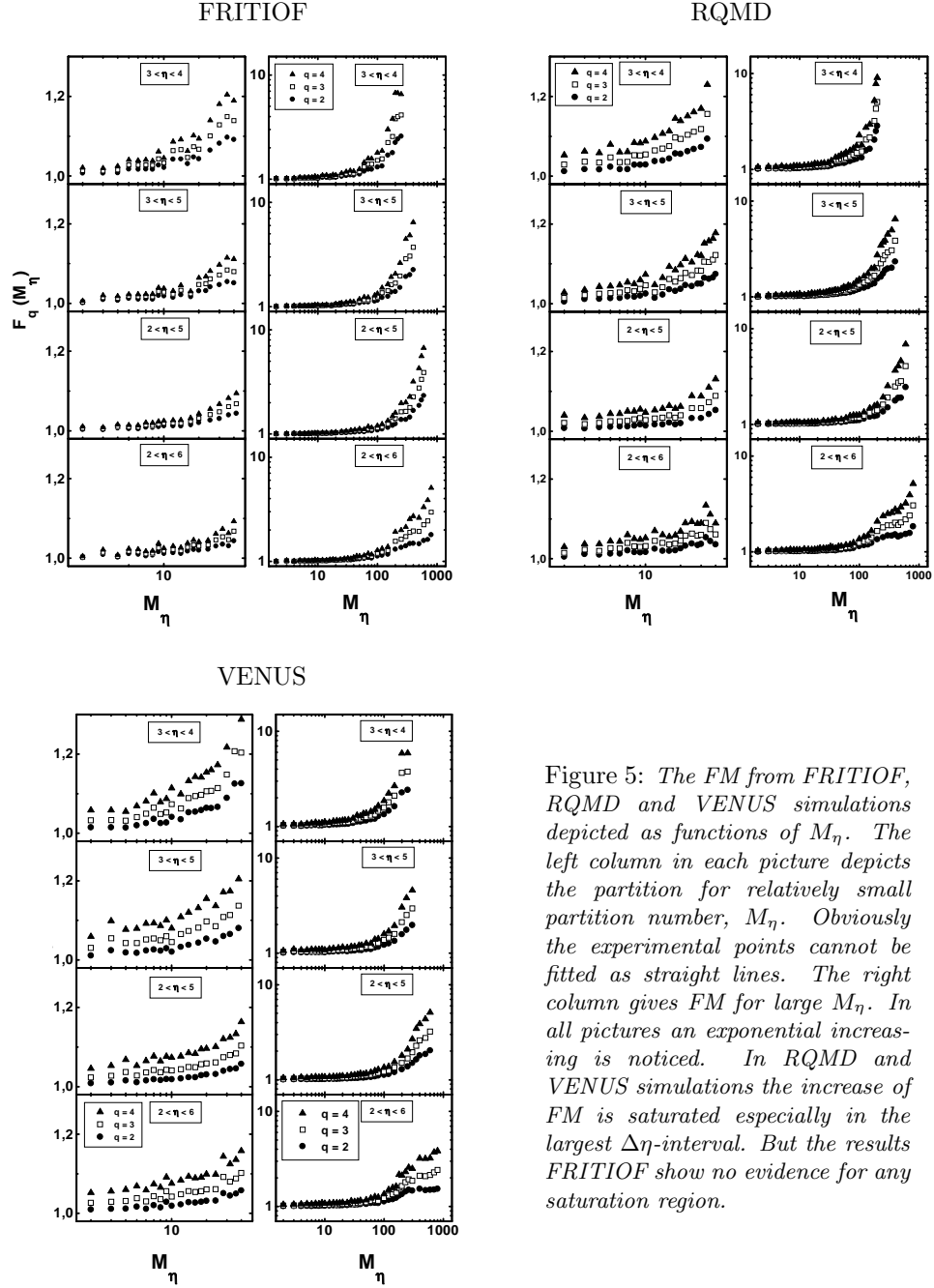


Figure 5: The FM from FRITIOF, RQMD and VENUS simulations depicted as functions of M_η . The left column in each picture depicts the partition for relatively small partition number, M_η . Obviously the experimental points cannot be fitted as straight lines. The right column gives FM for large M_η . In all pictures an exponential increasing is noticed. In RQMD and VENUS simulations the increase of FM is saturated especially in the largest $\Delta\eta$ -interval. But the results FRITIOF show no evidence for any saturation region.

source for the discrepancies may be the physics of the phase-transition which has not been taken into account in any model.

4.1 Upwards increasing

Going back to the gigantic upwards enhancement of FM with large $M_{\{\eta|\phi\}}$. We would like to begin here with two points: First, the results published in [25], in which the authors claimed that there is no more increasing in FM in the regions beyond the limit $\delta\eta < 0.1$. In this present work, we clearly notice that FM still have an obvious linear increasing, even up to the partition width $\delta\eta \approx 0.02$ (see Fig. 1 and Fig. 2). Beyond this *narrow* bin size, the increasing of FM does not only get ahead, but it becomes exponential. Second, a reasonable explanation of the tremendous growth of FM for large $M_{\{\eta|\phi\}}$ may be based on the *short-range* conventional correlations [26], on the hadronic resonance and cluster decay [4, 5], on the Bose–Einstein correlation, etc. In the following is another reason for this exponential increase [27, 28]: Using trivial geometric model, each projectile nucleon interacts along the cylindrical tube in the target nucleus with more than one nucleon. Therefore, for each of these sub-nucleus interactions, there is a pseudo-rapidity distribution [27] with certain mid-rapidity depending on the typical characters of such interacting systems. It depends also on the corresponding cross section, which in turn depends on whether the *knock* takes place between nucleons in face-to-face or between *eclipsed* ones [29]. In addition to these sub-interactions, the secondary particles (first and/or higher generations) produced within the target material cause further interactions with each other and with the target and projectile materials. These secondary interactions produce additional pseudo-rapidity distributions with their own mid-rapidity centers. Therefore, for each of these *elementary* collisions, a *sub* pseudo-rapidity center can be achieved. The superposition of these elementary pseudo-rapidity values taken place in *sub*-intervals $\delta\eta$, in which the original intervals $\Delta\eta$ has been partitioned, makes the total *effective* partition number, M^{eff} , larger than M ($M^{\text{eff}} \gg M$) [27]. The reasons for these additional effects can summarize as the following:

1. The successive elementary collisions cannot completely be coincident with each others. Therefore the final summation of *sub* pseudo-rapidity centers ($\sum \delta\eta$) produces one distribution with many centers ($M^{\text{eff}} \gg M$).
2. Even in the *ideal* case: The superposition produces only one distribution with only one center ($M^{\text{eff}} = M$), its position has not to be coincident with the center of original one, $\Delta\eta$. In this case, $M^{\text{eff}} \neq M$.

Evidently, these facts are able to explain the exponential increasing of FM (see Fig. 9 later). The effects of M^{eff} cannot be neglected in such large interacting system like Pb+Pb, since the degree of upwards increasing strongly depends on the number of participating projectile nucleons and on the size of the target tubes [29].

4.2 Influence of γ conversion on 1D FM

The measured FM are expected to be partially influenced by the e^-e^+ -pairs produced by Dalitz decay and/or by γ -conversion. In [8], the probabilities of γ -

conversion in the emulsion and in the lead foil are calculated and found that the percentage of γ 's converting to electron-pairs in the lead foil is $\sim 1.71 \pm 0.1$ and in the emulsion is $\sim 0.48 \pm 0.06$. Taking the detector resolution and the possible space angles between such pairs into account, it is possible to estimate that $\geq 78\%$ of these electrons cannot be grabbed by MIRACLE Lab. In addition to this effect of *unresolved close pairs*, most of, if not all, the rest of these electrons are obviously included within the so-called 4% discrepancy (Section 2). Therefore, we could consider that there is a negligible effect of γ 's on 1D FM. Another argument to support this conclusion is coming out from the simulation processes. Through adding γ 's to FRITIOF for example, it was found [30]: First, the influence from the Dalitz decay is obviously negligible. Second, the influence from the γ -conversion is undersized, or at least, comparable with the quoted statistical acceptances. Therefore, we can conclude that both of Dalitz decay and γ -conversion have an infinitesimal effect on 1D FM, especially in the data retrieved by MIRACLE Lab.

5 Results in Multi-Dimensions

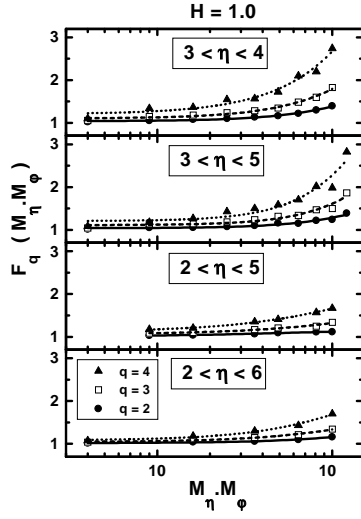


Figure 6: *FM* is performed here in two-dimensions simultaneously and then compared in the different $\Delta\eta$ -intervals. The partition process is performed for small number $M_\eta \cdot M_\phi$. Here, *FM* apparently increase faster than the 1D *FM* (Fig. 1 and Fig. 2) with the increasing of $M_\eta \cdot M_\phi$.

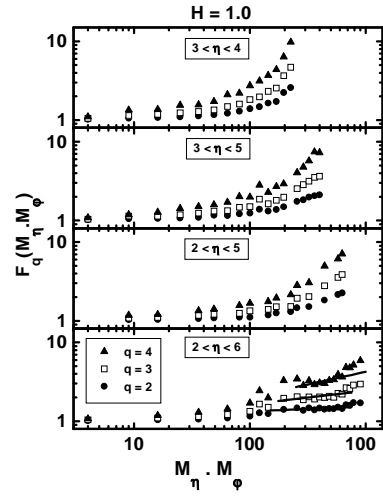


Figure 7: The same as in Fig. 6, but for large $M_\eta \cdot M_\phi$. We notice that the increasing of $\log F_q$ vs. $\log(M_\eta \cdot M_\phi)$ is upwards binding. Saturation regions as in Fig. 3 are observed here, especially in the largest $\Delta\eta$ -interval.

For clear understanding of the dynamics of the interaction and to investigate the

different reasons responsible for the multiplicity fluctuations and consequently to explain the power-law behavior at the final state of particle production, it is necessary to investigate FM in multi-dimensions (ϕ, p_t, η) [31]. Because of the absence of any external magnetic field during the emulsion exposure (Section 2), it is not possible to measure p_t . It remains only the two dimensions, η and ϕ [30]. For the multi-dimensional study of FM, we should first define the so-called *multi-dimensional* partition method. In next subsection, we introduce methods generally used for the two-dimensional partition.

5.1 Methods for two-dimensional partition

If the $\Delta\eta$ -interval is divided into the same number of bins as $\Delta\phi$, this method is called *self-similar* partition, i.e. the partition in certain dimension controls the method of the partition in the other one. Clearly, this method leads to total partition number of M^2 . A practical method to contemporaneously determine the partitions in two-dimensions is given by the so-called *Hurst-exponents* [32],

$$\mathcal{H}_{12} = \frac{\ln M_1}{\ln M_2}. \quad (12)$$

M_i ; $i = \{1, 2\}$ is the number of bins in i -th direction. If $\mathcal{H} = 1$, the two variables, η and ϕ , will be divided in a *self-similar* way. It was pointed out in [27, 33] and discussed in Section 4.1 that the superposition in η -dimension makes the *effective* partition number, $M_\eta^{\text{eff}} \gg M_\eta$. In the contrast, the superposition in ϕ -dimension makes no change at all, i.e. $M_\phi^{\text{eff}} = M_\phi$. These lead to $\mathcal{H}_{\eta\phi} = \ln M_\eta^{\text{eff}} / \ln M_\phi$, and

$$M_\eta^{\text{eff}} = e^{\mathcal{H}_{\eta\phi} \ln M_\phi}. \quad (13)$$

To study the possible *abnormal* behavior of FM with M , we should perform the analysis of FM for only one value of \mathcal{H} . Otherwise, the *observed* trend of the calculated FM will always be bending upwards [28], even if there is no fluctuation in the particle production. The upwards increasing of FM which is depending only on the partition method, can be weakened or totally removed (review Eq. (13)), if the exponents, \mathcal{H} , are given a suitable value. At this position, it is worthwhile to refer to the conclusion of [29] that the exponents, \mathcal{H} , applied in the particle production strongly depend on the energy and the mass of projectile and target.

5.2 Results in two-dimensions

F_q are drawn in Fig. 6 as functions of $M_\phi M_\eta$ for the different $\Delta\eta$ intervals. The partition processes have been performed in a *self-similar* way. The number of partition, $M_\phi M_\eta$, goes up to 100 for the different $\Delta\eta$ intervals, which enable us to study FM for different bin sizes. Here there is no restriction on the azimuthal angles ($\Delta\phi = 2\pi$ and $\delta\phi \in \{0, 2\pi\}$). In addition to the features concerning with the 2D-analysis, almost similar features as in Fig. 1 and Fig. 2 are observed

here, for example, the reduction of FM with the increasing of the considered $\Delta\eta$ -window and the large dispersions of FM with the decreasing of $\Delta\eta$. Obviously, the exponential increase of FM (Fig. 7) can be proportionally connected with $\Delta\eta$ -widths (see Fig. 3 and Fig. 4). The last could be understood, according to the facts that the increase of $\Delta\eta$ -width leads to an increasing of the size of the resulted bin $\delta\eta$. These observations support the assumption that the upwards increasing is to be explained due to the superposition of the non-coincident sub-intervals of the *sub* pseudo-rapidity values [27, 28] (Section 4.1). The partition numbers drawn here are smaller than the effective one, M^{eff} . According to Eq. (13), M^{eff} are functions of the Hurst-exponents \mathcal{H} (Section 5.1). Continue the partition process in Fig. 7, FM keep on the upwards increasing. As noticed in Fig. 3, saturation regions get formed in wide $\Delta\eta$ -intervals. In bottom picture of Fig. 7, the saturation curves are completely formed.

5.3 Influences of γ conversion on 2D FM

As discussed in Section 4.2, most of γ -conversions are expected to take place within the lead foil. The measuring system MIRACLE Lab is able to percolate the measurements from most of the tracks of electron-pairs (Section 2 and 4.2). Generally, the contributions of γ 's to multi-dimensional FM [30, 34] have to be taken into account. The features of MIRACLE Lab discussed above, for which we concluded that the effects of γ 's on 1D FM are to be neglected, are still valid also in 2D FM. Since we noticed that the interacting system, Pb+Pb, is intermittent in 1D FM (Fig. 1 to Fig. 4 and Fig. 6 to Fig. 7), we do not constrain to go through the estimation of γ 's in 2D [35] again. Another reason for this renounce is the fact that the estimation of γ 's is traditionally performed in the following way: Adding these processes to the used simulating code and comparing the experimental results with the simulated ones. If the last are able to describe the first, the fluctuations of γ 's are the responsible source for power-law behavior of FM [30, 34]. In our case, It is not needed to process this method, since the used measuring system is obviously able to filter the measurements from the electron-pairs.

6 Lévy Indices and Anomalous Dimensions

6.1 Ratios of intermittence exponents ϕ_q/ϕ_2

The relation between q - and second-order FM is given as:

$$\log F_q(M_{\{\eta|\phi\}}) = \frac{\phi_q}{\phi_2} \log F_2(M_{\{\eta|\phi\}}) + c_q, \quad (14)$$

ϕ_2 and ϕ_q are the slopes of the relations between $\log F_2(M_{\{\eta|\phi\}})$ and $\log F_q(M_{\{\eta|\phi\}})$ and the corresponding $M_{\{\eta|\phi\}}$. c_q are constant. From these two figures (also review Fig. 1 and Fig. 2 again), we notice that the exponents, ϕ_q , do not depend on $M_{\{\eta|\phi\}}$. Therefore, in practice the slope ratios, ϕ_q/ϕ_2 , can be deduced from the

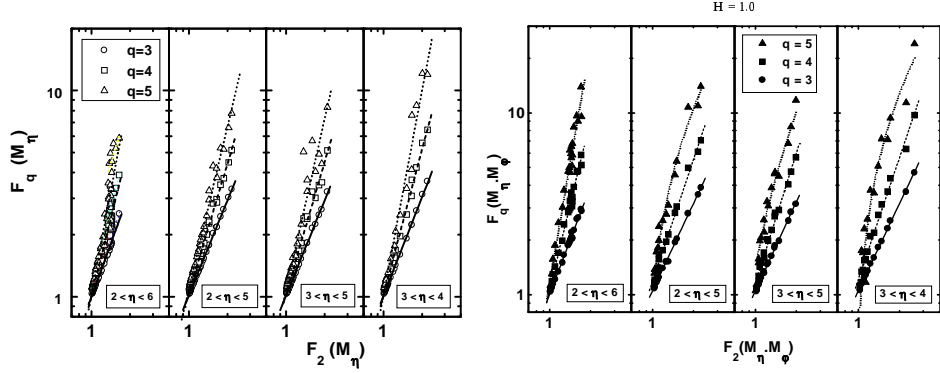


Figure 8: The dependence of q - on second-order FM in η -dimension is depicted. The lines represent the linear fitting of the experimental data. In Table 1, the fitting parameters are listed. We notice a positive dependence of F_q on F_2 for all $\Delta\eta$ -intervals in one- as well as in two-dimensions.

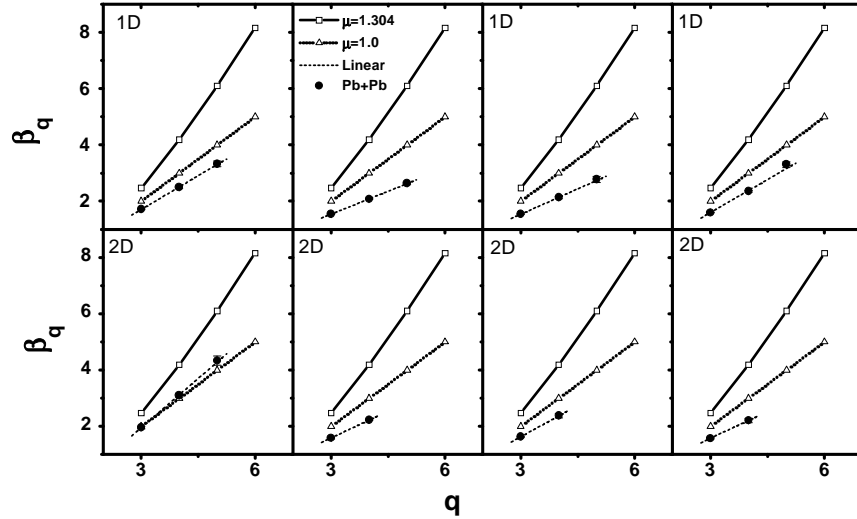


Figure 9: The ratios of intermittence exponents, $\beta_q = \phi_q/\phi_2$, given as functions of orders, q . The solid lines represent the fitting according to the relation (19). The fitting according to relation (17) is represented by the dotted lines. The conventional linear power fitting are given by the thin dash-lines. The experimental data are represented by the solid points.

Table 1: The fit parameters, ϕ_q/ϕ_2 and c_q , for the straight lines drawn in Fig. 8, left picture for 1D analysis, are listed here.

| η | q | value | η | q | value | | |
|----------------|---|-----------------|-------------------|----------------|-------|-----------------|-------------------|
| $3 < \eta < 4$ | 3 | c_3 | 0.003 ± 0.001 | $3 < \eta < 5$ | 3 | c_3 | 0.005 ± 0.001 |
| | | ϕ_3/ϕ_2 | 1.598 ± 0.009 | | | ϕ_3/ϕ_2 | 1.543 ± 0.007 |
| | 4 | c_4 | 0.006 ± 0.004 | | 4 | c_4 | 0.015 ± 0.003 |
| | | ϕ_4/ϕ_2 | 2.354 ± 0.033 | | | ϕ_4/ϕ_2 | 2.131 ± 0.035 |
| | 5 | c_5 | 0.007 ± 0.014 | | 5 | c_5 | 0.031 ± 0.011 |
| | | ϕ_5/ϕ_2 | 3.300 ± 0.102 | | | ϕ_5/ϕ_2 | 2.777 ± 0.110 |
| $2 < \eta < 5$ | 3 | c_3 | 0.006 ± 0.001 | $2 < \eta < 6$ | 3 | c_3 | 0.001 ∓ 0.001 |
| | | ϕ_3/ϕ_2 | 1.537 ± 0.004 | | | ϕ_3/ϕ_2 | 1.709 ± 0.023 |
| | 4 | c_4 | 0.017 ± 0.002 | | 4 | c_4 | 0.004 ± 0.005 |
| | | ϕ_4/ϕ_2 | 2.083 ± 0.015 | | | ϕ_4/ϕ_2 | 2.495 ± 0.056 |
| | 5 | c_5 | 0.035 ± 0.004 | | 5 | c_5 | 0.011 ± 0.013 |
| | | ϕ_5/ϕ_2 | 2.631 ± 0.039 | | | ϕ_5/ϕ_2 | 3.321 ± 0.129 |

relation $\log F_q(M_{\{\eta|\phi\}})$ vs. $\log F_2(M_{\{\eta|\phi\}})$. Fig. 8 depicts such relations for the orders, $q = \{3, 4, 5\}$. The lines represent the power fitting of the experimental data. Orders q increase, the slopes and their corresponding statistical errors get large. Comparisons between the fitting parameters in the different $\Delta\eta$ -intervals are summarized in Table 1. The results from the 2D-analysis are graphically illustrated in the right part of Fig. 8 and their corresponding parameters are listed in Table 2. From these two tables and by taking into account the different statistical errors in 1D and 2D, we can conclude that the corresponding slope ratios ϕ_q/ϕ_2 smoothly get larger for higher analysis dimension. In left picture in Fig. 8, *especially* in the largest $\Delta\eta$ -interval, $2 < \eta < 6$, we notice the existence of two separated regions. Each of them has been fitted and depicted as thin line. The suddenly increasing of the ratios, ϕ_q/ϕ_2 , at the boarder between these two regions measures the maximum amplitude of the saturation plateau of second-order FM (~ 1.5). At this point, $\phi_q/\phi_2 \rightarrow \infty$. The comparison between one- and two-dimensional FM requires to give \mathcal{H} -exponents, used to define the method of partition in two-dimensions, a suitable constant value. The value, $\mathcal{H} = 1$, obviously cannot overcome the effects of the superposition of the sub-intervals (*elementary collisions*). Therefore, we expect that FM exponentially increases for $\delta\eta \rightarrow 0$ (Fig. 7). This clearly explains the non-linear behavior of parts of the relations shown in the right picture in Fig. 8.

6.2 Physics of power-law behavior

As mentioned in Section 1 and discussed elsewhere [36, 37, 38], the sources responsible for the power-law behavior at the final state of particle production can be classified into two main groups:

1. *Self-similar processes*. By using Gaussian distributions [36], the ratios of q - to second-order intermittence exponents can be expressed as:

Table 2: The parameters, ϕ_q/ϕ_2 and c_q , from the linear power fitting drawn in Fig. 8, right picture for the 2D analysis, are given here.

| η | q | value | η | q | value |
|----------------|---|--------------------------|----------------|---|--------------------------|
| $3 < \eta < 4$ | 3 | c_3 ϕ_3/ϕ_2 | $3 < \eta < 5$ | 3 | c_3 ϕ_3/ϕ_2 |
| | | 0.024 ± 0.003 | | | 0.021 ± 0.003 |
| | | 1.579 ± 0.017 | | | 1.629 ± 0.023 |
| | 4 | c_4 ϕ_4/ϕ_2 | | 4 | c_4 ϕ_4/ϕ_2 |
| | | 0.084 ± 0.014 | | | 0.064 ± 0.012 |
| | | 2.213 ± 0.077 | | | 2.377 ± 0.083 |
| | 5 | c_5 ϕ_5/ϕ_2 | | 5 | c_5 ϕ_5/ϕ_2 |
| $2 < \eta < 5$ | 3 | c_3 ϕ_3/ϕ_2 | $2 < \eta < 6$ | 3 | c_3 ϕ_3/ϕ_2 |
| | | 0.021 ± 0.005 | | | 0.002 ∓ 0.006 |
| | | 1.592 ± 0.028 | | | 1.965 ± 0.040 |
| | 4 | c_4 ϕ_4/ϕ_2 | | 4 | c_4 ϕ_4/ϕ_2 |
| | | 0.072 ± 0.010 | | | 0.024 ± 0.012 |
| | | 2.226 ± 0.060 | | | 3.102 ± 0.081 |
| | 5 | c_5 ϕ_5/ϕ_2 | | 5 | c_5 ϕ_5/ϕ_2 |
| | | | | | 0.075 ± 0.025 |
| | | | | | 4.337 ± 0.170 |

$$\frac{\phi_q}{\phi_2} = \frac{d_q}{d_2}(q-1) = \binom{q}{2}. \quad (15)$$

As discussed in [37, 38], the implementation of Lévy index, μ [39], leads to:

$$\frac{d_q}{d_2} = \frac{q^\mu - q}{2^\mu - 2} \cdot \frac{1}{q-1}, \quad (16)$$

where μ has a continuous spectrum, $0 < \mu \leq 2$, (*region of Lévy stability*). Experimentally, EHS/NA22 collaboration [40] found that the index μ , in principle exceeds the upper boundary, 2. As we will see later, Lévy index within its restricted stability region evidently is not able to describe the experimental relations between d_q/d_2 and the orders q . Only for 2D FM in the rapidity region ranging from 2 to 6, we get a stable value, $\mu = +0.1$ (Fig. 10).

Relation (15) is evidently an approximation of anomalous ratios, d_q/d_2 . Obviously, this relation is not satisfactorily applicable in the distribution tails. Meanwhile relation (16) can effectively determine these tails. As given above, Lévy index has two boundaries (drawn in Fig. 10 as dotted lines):

- (a) $\mu = 2$ leads to $d_q/d_2 = q/2$ corresponding to *self-similar branching processes* represented by the well-known Gaussian distributions, and
- (b) $\mu = 0$ leads $d_q/d_2 = 1$ corresponding to *mono-fractal behavior* resulted from second-order phase-transition from QGP to hadron-gas [41].

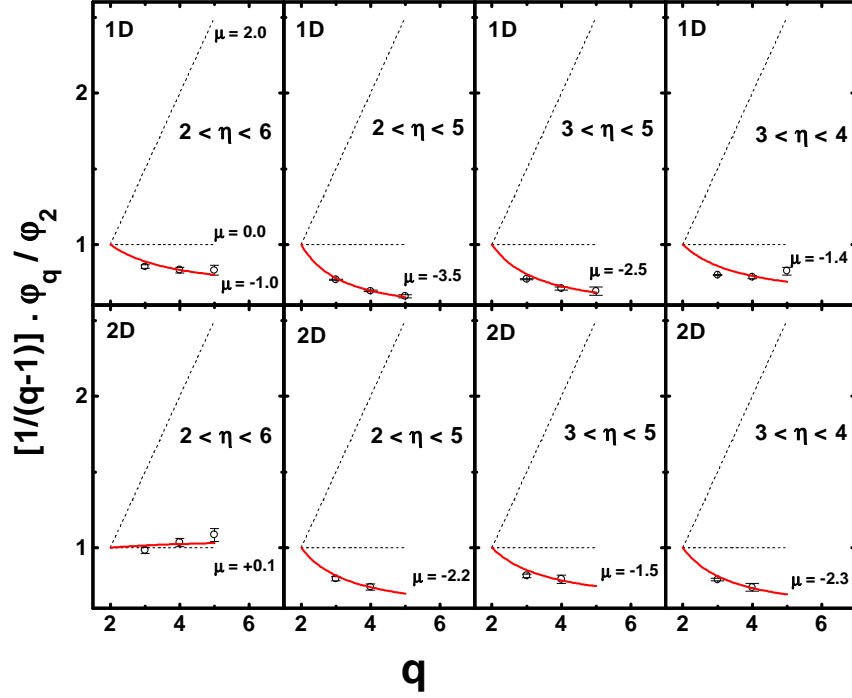


Figure 10: Dependencies of the anomalous dimension ratios, ϕ_q/ϕ_2 , with the orders, q , for the different $\Delta\eta$ -intervals and for the possible two dimension, η and ϕ . The dotted lines represent the two boundaries of Lévy stable region. The experimental results are represented by the open circles. The Solid lines are the solutions of Eq. (16) for the given μ -values.

Between these two limits, Eq. (15) is not valid and should be replaced by the relation (16).

2. If QGP indeed is to be produced in the relativistic heavy-ion collisions, the interacting system has to suffer *second-order phase-transition* during its space-time evolution. In this case the observed intermittence behavior (in form of power-scaling behavior) can be compared with the behavior in a system of mono-fractal (see Fig. 9 and Fig. 10),

$$\frac{\phi_q}{\phi_2} = q - 1. \quad (17)$$

Then we can conclude that the dependence of the ratios, ϕ_q/ϕ_2 , on the orders, q , reflects essential information about the reaction dynamics [36]. In following sections, we will study the different intermittence ratios in relation with the orders, q .

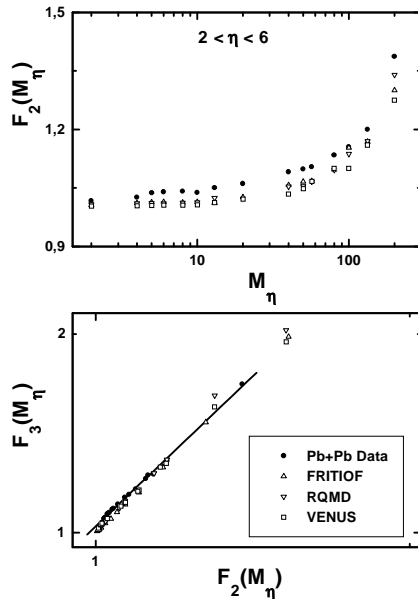


Figure 11: Comparison between the second-order FM and the partition number, M_η , for the experimental and simulated events (Section 2.1). The disagreement between the data and the three models becomes larger for larger M_η . In bottom part, the third-order FM are given as functions of the second-order ones for the same data set as in the top picture. The line represents the linear power fitting of the experimental data. Generally, we conclude that non of the three models is able to describe the experimental results.

6.3 Relations between ϕ_q/ϕ_2 and the orders q

In form of a power-law, relation (14) can be re-written as:

$$F_q \propto F_2^{\beta_q}; \quad \beta_q \equiv \phi_q/\phi_2. \quad (18)$$

It is clear to recognize that the critical powers, β_q , are independent on the partition process or on the analysis dimension. This power-law is valid in one as well as in multi-dimensions [38]. In [42], the predicted second-order phase-transition in heavy-ion collisions has been simulated by using a specific form of Ginzburg–Landau model [43]. It has been found that critical exponents, β_q , are independent on the temperature, T , just below the critical one, T_c . Therefore, the behavior of β_q effectively characterizes the phase-transition to coherent light and also its aftereffects

$$\beta_q = (q - 1)^\nu; \quad \nu = 1.304. \quad (19)$$

In our case, the aftereffects is the ratios, ϕ_q/ϕ_2 , or fundamentally the fluctuations in the particle production. ν are not looking like the conventional critical

indices describing only the behavior of quantities near the critical point. In addition to this, they are independent on the details of the interacting system and therefore can effectively characterize the behavior of all measurable quantities [42] (ϕ_q/ϕ_2 , etc).

Figure 9 describes the powers, β_q , as functions of the orders, q . As given before, β_q can directly be determined from the slopes of straight-line portions in Fig. 8. The slopes are given in Tables 1 and 2 for 1D and 2D, respectively. The lines with empty squares are the fitting according to the relation (19). Almost the same process, but for $\nu = 1.0$, is represented by the dash-lines. The value $\nu = 1.0$ in Eq. (17) is originally obtained from the intermittent behavior of 2D Ising-model [44] and also from the thermal second-order phase-transition (Section 6.1). From Fig. 9, we also notice that the first fitting is unable to describe the experimental data. Although the second one results lines close to the experimental points, it remains unable to completely predict the experimental results. Only, 2D-analysis in the region, $2 < \eta < 6$, produces one line coincident with the points representing the experimental data (solid points).

6.4 Relations between d_q/d_2 and the orders q

Figure 10 depicts the ratios, d_q/d_2 , in dependence with the orders, q , for the different $\Delta\eta$ -intervals. The relations between the anomalous and Rényi dimensions are given in Section 3.1. Virtually, this figure can be used to distinguish between the two possible sources of the intermittent behavior discussed in Section 6.2. As we can see, only Lévy indices ranging from -1.0 to -3.5 can fit our experimental data. The most acceptable value, $\mu = +0.1$, is obtained for 2D FM in the largest $\Delta\eta$ -interval. The reasons and interpretations for this monofractal behavior ($\mu \rightarrow 0$, Eq. (16)) we will discuss later. Again, the predictions of Eq. (17) are exactly the lower Lévy boundary, where the line $\mu = 0$ is.

7 Remarks and Final Conclusions

The following remarks have to be considered for the *evidence* of the thermal phase-transition noticed in this article:

1. FM have to be re-performed for higher orders and dimensions. Such a way, we get more lines for Fig. 9 and Fig. 10, which might support the observation of thermal phase-transition. For the same reason, more measurements are also required.
2. 2D FM have to be re-investigated by using other values of \mathcal{H} . Such a way, we can investigate the scaling-law behavior of FM away from the *non-canonical* effects stemming only from the partition method itself (Section 5.1).
3. $\Delta\eta$ -windows have to re-determined to specify the regions which fulfill the requirement of Lévy stability. The non-considered interval might include

leading baryons with pseudo-rapidity values close to that of the projectile nucleons. In that case, most of particles are of course fragmentations. Therefore, they behave differently than the produced ones (π 's).

4. In forthcoming steps, more weight should be given to the smaller intervals and to the dynamics of the interaction. The last could be studied by using the *event-by-event* fluctuations. Generally, the analysis of single events with huge multiplicity enable us to study different physics: geometry of interaction, space-time evolution, two-particle correlation functions, microscopic and thermodynamic collisions, QCD fluctuations, phase-transition, etc. [45].

Even, if we could include *leading*-particles, it is still early to dwell on ultimate conclusion. Since these *non-produced* particles may uncommonly comport as the produced ones, π 's. Although this conclusion could, in the one hand, be a uproarious one, especially in light of the remarks stated before, in the other hand, we cannot totally neglect the demonstrative evidence noticed in Fig. 10 and Fig. 11. Experimentally — in only one of $\Delta\eta$ regions — we have a stable Lévy index, $\mu = +0.1$ (Fig. 9 and Fig. 10). This positive *small* value is standing as a signature for the thermal phase-transition [37]. The other values, $\mu < 0$, indicate that Lévy indices cannot effectively distinguish between thermal and non-thermal branching processes.

The stable value, $\mu = +0.1$, is obtained from the two-dimensional analysis of the largest $\Delta\eta$ region. Within this region, the effects of the superposition in η -dimension are much smaller than that in other η -intervals [29] (Section 4.1). Within it, there are also *non-produced* particles, which in contrast to the produced particles, are not sensitive to the phase-transition. As mentioned above, more measurements, event-by-event analysis and higher dimensions are highly required to demonstrate such power-law scaling behavior and then to confirm the evidence of the thermal phase-transition.

Acknowledgement

This work is financially supported by the Deutscher Akademischer Austauschdiest (DAAD). We are very grateful to E. Stenlund and all colleagues of EMU01 collaboration for the helpful discussions and the kind assistance. Especially that they allowed us the use of part of our collaborative experimental data for this work. A.M.T. would like to thank F. Pühlhofer for the continuous support.

References

- [1] T.H. Burnett et al., *Phys. Rev. Lett.* **50** (1983) 2062.
- [2] A. Białas and R. Peschanski, *Nucl. Phys.* **B273** (1986) 703.
- [3] A. Białas and R. Peschanski, *Nucl. Phys.* **B308** (1988) 857.

- [4] P. Curruthers, E. Friedlander, C. Shih and R. Weiner, *Phys. Lett.* **222** (1989) 487.
- [5] A. Capella, K. Fialkowski and A. Krzywicki, *Phys. Lett.* **B230** (1989) 149.
- [6] M. Biyajima, *Prog. Theor. Phys.* **66** (1981) 1378; M. Gyulassy, S. Kaufmann and L. Wilson, *Phys. Rev.* **C20** (1979) 2267; D. Seibert, *Phys. Rev. Lett.* **63** (1989) 136; I. Derado, G. Jancso and N. Schmitz, *Z. Phys.* **C56** (1992) 553; Yu.M. Sinyukov and B. Lörstad, *Z. Phys.* **C61** (1994) 587; T. Wibig, *Phys. Rev.* **D53** (1996) 3586.
- [7] N. Neumeister et al., *Z. Phys.* **C60** (1993) 633.
- [8] A.M. Tawfik, *Kritische Studien zu der Teilchenkorrelationen und den Signaturen des Phasenübergangs in zentralen Blei-Blei-Stößen bei 158 GeV/c pro Nukleon*, Tectum-Verlag, Marburg, 1999, in German.
- [9] E. Ganssauge and A.M. Tawfik, *Nucl. Instr. Methods* **A416** (1998) 136.
- [10] A.M. Tawfik and E. Ganssauge, *Comput. Phys. Commun.* **118** (1999) 49.
- [11] EMU01 collaboration, M.I. Adamovich et al., *Phys. Lett.* **B390** (1997) 445.
- [12] W. Yuangfang and L. Lianshou, *Z. Phys.* **C53** (1992) 273.
- [13] H. Pi, *Comp. Phys. Commun.* **71** (1992) 173; B. Andersson, G. Gustafson and H. Pi, *Z. Phys.* **C57** (1993) 485.
- [14] H. Sorge, *Phys. Rev.* **C52** (1995) 3291.
- [15] K. Werner, *Phys. Rep.* **232** (1993) 87.
- [16] L. Van Hove, *Ann. Phys.* **192** (1989) 66.
- [17] N.M. Agababyan et al., *Z. Phys.* **C59** (1993) 195.
- [18] R. Peschanski, Talk at the Workshop on “Intermittency in High Energie Collisions”, Santa Fe, USA, March 1990.
- [19] R.C. Hwa, *Nucl. Phys.* **B328** (1989) 59.
- [20] C.B. Chiu and R.C. Hwa, *Phys. Lett.* **B236** (1990) 466.
- [21] R. Peschanski, *Int. J. Mod. Phys.* **A6** (1991) 3681.
- [22] P. Lipa and B. Buschbeck, *Phys. Lett.* **B223** (1989) 465; W. Kittel, Invited Review at the 4th Annual Seminar on “Nonlinear Phenomena in Complex Systems”, Minsk, Belarus, Feb. 6-9, 1995.
- [23] B. Buschbeck, P. Lipa and R. Peschanski, *Nucl. Phys.* **B215** (1988) 788.
- [24] A.M. Tawfik, in press.

- [25] EMU01 collaboration, M.I. Adamovich et al., *Phys. Rev. Lett.* **65** (1990) 412.
- [26] P. Carruthers and I. Sarcevic, *Phys. Rev. Lett.* **63** (1989) 1562.
- [27] EMU01 collaboration, M.I. Adamovich et al., *Z. Phys.* **C76** (1997) 659.
- [28] W. Yuanfang and L. Lianshou, *Phys. Rev. Lett.* **70** (1993) 3197; L. Lianshou, H. Yuan and D. Yue, *Phys. Lett.* **B388** (1996) 10; L. Lianshou, Z. Yang and W. Yuanfang, *Z. Phys.* **C69** (1996) 323; L. Lianshou, Z. Yang and D. Yue, *Z. Phys.* **C73** (1997) 535.
- [29] A.M. Tawfik, *Inelastic Interaction of ${}^6\text{Li}$ with Emulsion Nuclei at 4.5 AGeV/c incident Momentum*, Assiut University, Egypt, 1993.
- [30] EMU01 collaboration, M.I. Adamovich et al., *Nucl. Phys.* **B388** (1992) 3.
- [31] W. Ochs, *Phys. Lett.* **B247** (1990) 101.
- [32] B.B. Mandelbrot, *Die fraktale Geometrie der Natur*, 1. Sonderausgabe, Birkhäuser, Basel, 1991, in German.
- [33] L. Van Hove, *Phys. Lett.* **28B** (1969) 429; L. Van Hove, *Nucl. Phys.* **B9** (1969) 331.
- [34] WA80 Collaboration, R. Albrecht et al., *Phys. Rev.* **C50** (1994) 1048.
- [35] W. Ochs, *Acta Phys. Polon.* **B22** (1991) 203.
- [36] A. Białas and R.C. Hwa, *Phys. Lett.* **B253** (1991) 436.
- [37] Ph. Brax and R. Peschanski, *Phys. Lett.* **B253** (1991) 225; Y. Zhang, L. Liu and Y. Wu, *Z. Phys.* **C71** (1996) 499.
- [38] W. Ochs, *Z. Phys.* **C50** (1991) 339.
- [39] B.W. Gnedenko and A.N. Kolmogorov, *Grenzverteilungen von Summen unabhängiger Zufallsgrößen*, Akademie-Verlag Berlin, 1960, in German.
- [40] EHS/NA22 collaboration, N. Agababyan et al., *Z. Phys.* **C59** (1993) 405.
- [41] S. Hegyi, *Phys. Lett.* **B318** (1993) 642.
- [42] R.C. Hwa, M. Nazirov, *Phys. Rev. Lett.* **65** (1992) 741.
- [43] E.M. Lifshitz and L.P. Pitaevskii, *Statistical Physics*, Pergamon, Oxford, 1980.
- [44] H. Satz, *Nucl. Phys.* **B326** (1989) 613; B. Bambah and H. Satz, *Nucl. Phys.* **B332** (1990) 629.

- [45] H. Appelshäuser et al., *Phys. Lett.* **B459** (1999) 679; M. Stephanov, K. Rajagopal and E. Shuryak, hep-ph/9903292, unpublished; A. Capella, E.G. Ferreira and A.B. Kaidalov, hep-ph/9903338 unpublished; G. Odyniec, *Acta Phys. Polon.* **B30** (1999) 385; M.A. Stephanov, *Proceeding of the 14-th International Conference on “Ultrarelativistic Nucleus-Nucleus Collisions”*, QM '99, Torino, Italy, 10–15 May 1999.